Surface segregation in CuPt alloys by means of an improved modified embedded atom method

M. Schurmans,[1,*] J. Luyten,[1] C. Creemers,[1] R. Declerck,[2] and M. Waroquier[2]
[1]*Department of Chemical Engineering, K.U. Leuven, Willem de Croylaan 46, B-3001 Leuven, Belgium*
[2]*Center for Molecular Modeling, Laboratory of Theoretical Physics, Ghent University, Proeftuinstraat 86, B-9000 Gent, Belgium*
(Received 2 March 2007; revised manuscript received 28 June 2007; published 26 November 2007)

We present a procedure to investigate surface structures in CuPt alloys by combining the modified embedded atom method (MEAM) and the cluster expansion method (CEM). While the MEAM provides structural information for the description of extended anisotropic defects, the CEM improves the ability to correctly reproduce the relevant ground state structures in agreement with *ab initio* data. The procedure is validated with the reproduction of surface energies of pure Cu and Pt, the prediction of T_C for order-disorder transitions, the surface and segregation energies in ordered CuPt alloys, and Monte Carlo (MC) simulations of temperature-dependent surface segregation profiles. A complete MEAM-CEM/MC study of the surface segregation in Cu_3Pt, CuPt, and $CuPt_3$ alloys is presented, engaging only 11 composition- and volume-independent alloy-specific parameters. Results are critically compared with experimental data from literature and with an independent set of *ab initio* periodic density functional theory calculations.

DOI: 10.1103/PhysRevB.76.174208 PACS number(s): 31.15.Ct, 68.35.Dv, 81.30.Hd, 61.66.Dk

I. INTRODUCTION

The physical and chemical behaviors at metal alloy surfaces are crucial for several technological processes. CuPt alloys show interesting catalytic properties, among which is an improved activity and selectivity for CO oxidation and hydrocarbon reactions with respect to pure Pt.[1–3] A detailed knowledge of the energetic interactions at the metallic surfaces, as well as the effect of alloying, is necessary to improve our understanding of these phenomena. In addition to a broad range of experimental techniques that can be used to examine the surface structure, composition, and ordering, several reliable theoretical methods are nowadays also available. The increased computational capacity makes an accurate *ab initio* calculation of the energies of real and hypothetical atomically ordered systems feasible. It has also been shown that a combination of statistical mechanics and parametrized interatomic potentials, e.g., embedded atom method[4] (EAM), modified EAM[5] (MEAM), Bozzolo-Ferrante-Smith[6] (BFS) method, bond order potentials,[7] and cluster expansion method[8,9] (CEM), fitted in a consistent set of *ab initio* data, are able to describe (partly) disordered systems within acceptable time limits. The accuracy that can be expected from calculations using these semiempirical methods depends on the size and level of theory of the *ab initio* training set data used for fitting the interatomic potentials[10] and even on the predictive power of the potentials[11,12] themselves. The main purpose of this work is to reproduce the equiatomic $L1_1$ CuPt ground state with MEAM so that MEAM calculations are more widely applicable and in better agreement with the first principles benchmarks.

II. METHODOLOGY

The procedure proposed in this work consists of a MEAM description in combination with the flexible parametrization of CEM, thereby making optimal use of the synergism of both methods. This procedure has been validated on CuPt: MEAM introduces structural information, capable of describing extended defects while CEM correctly reproduces the ground state of the equiatomic $L1_1$ CuPt. The surface energy of ordered CuPt alloys as predicted by MEAM-CEM is then assessed by *ab initio* values obtained from periodic density functional theory (DFT) calculations that were not used in the training set. Finally, we will predict the equilibrium surface composition and ordering in the CuPt system with this MEAM-CEM method and Monte Carlo (MC) simulations, and we will compare our estimates with available experimental evidence.

MEAM was originally developed by Baskes,[5] who extended the EAM[4] to account for directional bond characteristics. The interatomic MEAM potentials have been proven to accurately describe a number of properties that explicitly depend on the interatomic distances (e.g., fcc-bcc transition and bulk modulus). This explains its many successful applications in structural calculations,[13] molecular dynamics,[14] surface MC simulations,[15,16] etc. However, the number of interaction parameters in MEAM is limited, and by design, the potential generally maximizes the number of nearest-neighbor bonds between different atomic species. This is a serious drawback in the description of CuPt as the equiatomic alloy orders in the $L1_1$ rather than the $L1_0$ structure. Moreover, in general, CuPt is not an exception by showing non-nearest-neighbor based ground states. Based on extensive *ab initio* investigations,[17,18] complicated ground states in ordered transition metal alloys are nowadays emerging rather as the rule. A CEM correction to MEAM can then also help to take into account the more complicated ground states.

In this paper, we will not present a full CuPt ground state search, but we will illustrate that a combination of MEAM with even a basic version of the CEM substantially improves the validity of the MEAM. The interatomic interaction parameters derived from the CEM generate MEAM-CEM energies, leading to a better reproduction of the heat of formation of a number of atomically ordered alloys. A similar correction has recently been proposed to adjust the nonlinear attractive interactions in the BFS method.[12] In the present paper, we propose an algorithm that is illustrated in Fig. 1.

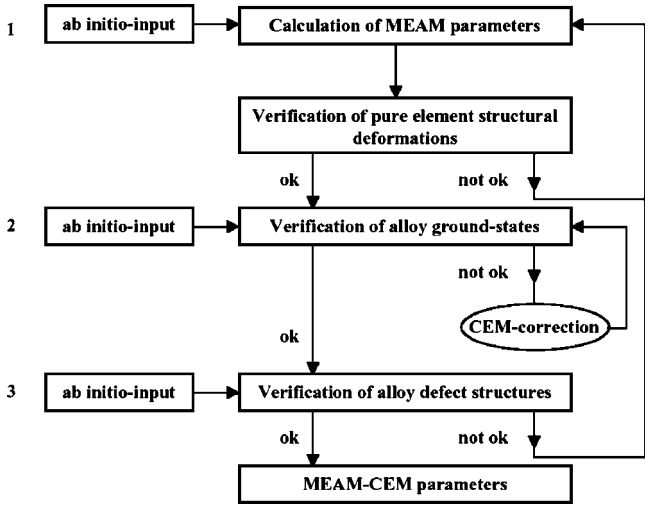

FIG. 1. Scheme for improving MEAM calculations with a CEM correction.

First, we determine MEAM parameters from *ab initio* data (step 1), and then validate them by comparing structural deformations (e.g., bulk distortions, vacancies, and surfaces) and alloy ground state predictions with those predicted by *ab initio* calculations and experiments (step 2). In this process, all the available MEAM parameters are optimized. Step 2 includes the calculation of the heat of formation of bulk alloys as a function of interatomic distance and a number of bulk MC simulations both below and above the critical temperature T_C for an order-disorder transition. If this step reveals the prediction of an incorrect ground state and if this cannot be corrected within the valid boundaries of the MEAM parameters, a number of cluster interactions are selected to correct the MEAM ground state prediction. The ground state is then again verified, and, if necessary, more cluster interactions are added until a completely satisfactory reproduction of the relevant ground state structures is obtained. Finally, in step 3, the resulting MEAM-CEM method is tested by calculating (mainly alloy) structural deformations. In this paper, step 3 includes MC simulations of low index surfaces and energy calculations of ordered CuPt alloy surfaces that are compared to DFT calculations and experiments.

The procedure comprises two completely different sets of DFT calculations. A first type of periodic DFT calculations has been performed on a training set determining the MEAM and CEM parameters. This fitting procedure is tested by calculating surface properties of CuPt alloys (e.g., correct prediction of surface terminations of ordered CuPt alloys) with the MEAM-CEM and comparing them with results from a different DFT study. The two different sets of DFT calculations were performed independently using two different calculation packages in order to obtain maximally unbiased information. DFT-PW91 (Ref. 19) gradient-corrected functional calculations were performed on the training set using the Vienna *ab initio* simulation package (VASP).[20,21] On the other hand, the test set comprises DFT local density approximation (LDA)[22] and DFT-PW91 calculations performed with the QUANTUM-ESPRESSO (QE) package.[23] In this way, the test set helps to understand the surface segregation profiles obtained from MEAM-CEM. The use of two different approaches in the test set strengthens the evidence about the predicted stability of surface terminations of ordered CuPt alloys.

The ground state structures were calculated in VASP and QE while imposing periodic boundary conditions in the three spatial directions. Ultrasoft pseudopotentials[24] are used to describe the electron-ion interaction. The energy of all structures was converged to within 0.001 eV/atom with respect to the plane wave cutoff energy and the number of k points sampling the first Brillouin zone. In a variable cell relaxation, the equilibrium energy and structure of the lattices Cu_3Pt ($L1_2$), CuPt ($L1_0$), CuPt ($L1_1$), and $CuPt_3$ ($L1_2$) were determined. Together with the equilibrium energy per atom of pure Cu (fcc) and Pt (fcc), this allows us to calculate the sublimation energy ΔH^{sub} per atom of each of the constituents and the total heat of formation ΔH^f of the ordered bulk alloys. In the DFT-PW91 (VASP) calculations of CuPt alloys, relaxation effects are constrained so as to maintain the fcc structure enabling a straightforward determination of the MEAM parameters. No such constraint was imposed in the calculation of the test set with QE. This additional degree of freedom only affects the CuPt $L1_0$ lattice, which is subject to a tetragonal distortion that lowers the CuPt $L1_0$ formation energy ΔH^f by 0.018 eV/atom.

The next section provides more details regarding the determination of MEAM parameters. Section III A presents the MEAM parametrization of pure Cu, pure Pt, and CuPt interactions. Section III B gives a brief overview of the description of structural defects with the CEM-formalism. In Sec. IV, an improvement of MEAM ground state predictions is achieved by means of a CEM correction. Finally, the MEAM-CEM algorithm is implemented in order to study and discuss the surface segregation at the three low index single crystal surfaces of CuPt alloys (Secs. V and VI).

III. PARAMETRIZATION OF MEAM AND CEM FOR THE DESCRIPTION OF ALLOY SURFACES

A. Modified embedded atom method description of CuPt alloys

In Ref. 10, Luyten *et al.* described a new and more consistent way of fitting MEAM parameters to DFT calculations and applied the method to describe surface segregation in Cu_3Pt. In that work, all MEAM interactions are restricted to nearest neighbors. Table II in Ref. 10 demonstrates that, even with a limited set of included interactions, MEAM successfully predicts the energies of a wide range of isotropic and anisotropic structural deformations of pure Cu and pure Pt. The bulk heat of formation, the equilibrium lattice parameter, and the bulk modulus of a "reference" structure, Cu_3Pt ($L1_2$) correspond to three MEAM alloy parameters. These material properties of the reference structure are therefore exactly reproduced. A good agreement with the heats of formation of three additional ground state ordered structures, CuPt ($L1_0$), CuPt ($L1_1$), and $CuPt_3$ ($L1_2$), is obtained by including another group of two MEAM parameters. However, despite

TABLE I. MEAM and DFT-PW91 (VASP) predictions for the equilibrium NN distance (R_0) and heat of formation (ΔH^{form}) for various ordered CuPt compounds.

	R_0 (Å)		ΔH^{form} (eV/atom)	
	MEAM	DFT-PW91 (VASP)	MEAM	DFT-PW91 (VASP)
Cu_3Pt ($L1_2$)	2.65	2.65	−0.140	−0.143
CuPt ($L1_0$)	2.71	2.72	−0.219	−0.124
CuPt ($L1_1$)	2.73	2.72	−0.199	−0.153
$CuPt_3$ ($L1_2$)	2.77	2.76	−0.186	−0.118

this additional set, the relative stability of the different ordered structures remains unaltered. Reference 10 lists all the MEAM parameters for the CuPt system determined in this way. The present paper adopts the same numerical values of the MEAM parameters. Predictions of the heat of formation and the equilibrium interatomic distance of a number of CuPt alloys with DFT-PW91 (VASP) and MEAM calculations are presented in Table I.

One of the peculiarities of the CuPt system is the existence of the $L1_1$ structure at the equiatomic composition, with planes of pure Pt and pure Cu alternating in the (111) direction. According to the phase diagram,[25] this $L1_1$ structure is stable up to 1089 K. DFT-PW91 (VASP) calculations at 0 K predict the correct ground state configuration, the $L1_1$ structure being 0.029 eV/atom more stable than the unrelaxed $L1_0$ structure (see Table I). MEAM, on the contrary, predicts a larger stability for CuPt $L1_0$. The latter is favored by eight bonds between unlike nearest neighbors versus only six in the $L1_1$ structure. The larger MEAM stability of CuPt $L1_0$ (Table I) is triggered by the too exothermic interactions between nearest-neighbor CuPt pairs as compared to further ranging interactions. Although $L1_0$ is the most stable equiatomic compound in more binary alloys than $L1_1$,[25] both theoretical and experimental techniques have found a stable $L1_1$ ground state for equiatomic CuPt, and the standard MEAM procedure fails to reproduce this. The energy difference between the two compounds ($L1_1$ versus $L1_0$) may be rather small, but as the MEAM parameters have been determined by a fitting procedure with a training set constructed by DFT-PW91 (VASP) data, one might at least expect that MEAM would reproduce the same ground state configuration. The results of this paper indicate that this has no consequences if MEAM is applied to Cu_3Pt. However, when investigating the equiatomic CuPt alloy, equilibrium MEAM/MC simulations automatically refer to the incorrect $L1_0$ ground state. MEAM/MC simulations of the equiatomic CuPt alloy then evolve to a bulk composition profile oscillating in the (100) direction with alternating layers of pure Cu and pure Pt. Since the $L1_1$ ordered alloy has stoichiometric layers in the (100) direction, one cannot expect to accurately describe segregation in equiatomic CuPt alloys with the current version of MEAM.

B. Cluster expansion method

At this moment, CEM provides the most consistent and versatile framework for including an arbitrary amount of total energy calculations from first principles in the parametrization of a multicomponent system on a lattice structure.[26] CEM[27] calculates the heat of formation of multicomponent lattice systems with the following Ising cluster expansion:

$$\Delta H^f_{CEM} = J_0 + \sum_{sites} J_i \hat{S}_i + \sum_{pairs} J_{ij} \hat{S}_i \hat{S}_j + \sum_{triplets} J_{ijk} \hat{S}_i \hat{S}_j \hat{S}_k + \cdots = \sum_{\alpha} J_\alpha \sigma_\alpha, \quad (3.1)$$

where $\hat{S}_i$ are spin variables with a value of ±1 depending on the occupation of the corresponding sites by an atom A or B. α runs over all symmetry-equivalent figures in the lattice, and the interaction energies J_α are determined[28,29] either via empirical fits, via perturbation theory, via direct inversion, or via a least-squares method. The cluster expansion provides a complete basis,[27] and hence the energy of different configurations can be reproduced with any desired degree of accuracy, provided that enough different symmetry-equivalent figures α are taken into account. A limited number of interactions are usually selected in advance, but, recently, genetic algorithms were used to map *ab initio* results to model Hamiltonians.[30,26]

As far as *local* structural variations and relaxations are concerned, the description in CEM varies from completely neglecting relaxations over determining volume-dependent interaction energies $J_\alpha(V)$ to adding a volume-dependent reference energy E_{ref} [e.g., $E_{ref}=\Omega(V)x(1-x)$]. For the extension to long period superlattices, the concept of constituent strain cluster expansion was developed.[8] Recently, pair potentials dependent on interatomic distances were combined with CEM and have improved ability to model phase stability in bulk alloys.[31] These pair potentials are reported to take into account the effect of local structural variations. To our knowledge, accounting for extended defects such as surfaces has hitherto not been described by structural additions to the CEM.

If, on the other hand, an extended defect is considered as a new degree of freedom, it becomes possible to describe the occupation of the lattice sites in the neighborhood of this defect with a CEM description of that specific structure.[29] The same accuracy can then be obtained as in CEM bulk calculations. However, the parametrization of each additional degree of freedom comes at a computational cost that is similar to an additional ground state search.

As an alternative to the large amount of additional *ab initio* calculations that are needed to describe surfaces with pure CEM only, we propose to combine the ability of MEAM to accurately deal with structural defects in alloys, such as lattice distortions, vacancies, and surfaces, with the versatility of CEM that, by design, is able to predict the bulk alloy ground states with an accuracy comparable to the *ab initio* method by which it was parametrized.

IV. MODIFIED EMBEDDED ATOM METHOD-CLUSTER EXPANSION METHOD

The difference between the heat of formation of a number of relaxed ordered alloy configurations predicted with *ab ini-*

tio methods and with MEAM is expressed by a parameter Δ as follows:

$$\Delta(\text{config}) = \Delta H^f_{ab\ initio}(\text{config}) - \Delta H^f_{MEAM}(\text{config}). \tag{4.1}$$

By definition, Δ is zero if the configuration was used as the reference structure in the MEAM parametrization. In situations where Δ is of the same order of magnitude as the energy difference between the two most stable configurations, MEAM can predict the wrong alloy structure as the ground state. The competition between the $L1_1$ and $L1_0$ structures for CuPt, described in the previous section, provides a good example of this problem. This is not surprising as the amount of alloying interactions that are included in the standard MEAM is limited. The idea of the method we propose is to calculate Δ for a number K of atomically ordered configurations and to express these Δ's as a correction energy ΔH^c_{CE} in an expansion of various cluster interactions,

$$\Delta(\text{config}_k) = \Delta H^c_{CE}(\text{config}_k) = \sum_\alpha J_\alpha \sigma_\alpha \quad \text{for } k = 1,2,\ldots,K. \tag{4.2}$$

In order to keep the parametrization effort of the same degree of complexity as in commonly used MEAM versions, the cluster interactions in the expansion described in this paper are all volume independent. Moreover, they are restricted to null (α=0) clusters, point (α=1) clusters, nearest-neighbor (NN) (α=2) and second NN (α=5) pair clusters, and NN triangle (α=3) and NN tetrahedron (α=4) clusters. By construction, the original MEAM parameterization already provides an accurate description of pure Cu, Pt, and $L1_2$ Cu_3Pt. Nevertheless, these structures are also included in the CEM parametrization to ensure that the CEM parameters do not perturb the already established MEAM precision. The inclusion of $L1_0$ and $L1_1$ CuPt leads to a correct ground state description of the equiatomic alloy. For symmetry reasons, $L1_2$ $CuPt_3$ is included as well. The interaction parameters J_α are now calculated by matrix inversion[32] and are based on the difference between MEAM and *ab initio* energies for the six ordered configurations. Before introducing the matrix that links the interaction parameters J_α with the correction energies $\Delta(\text{config}_k)$, a correlation function $\bar{\Pi}_\alpha$ is defined for each class α of symmetry-equivalent figures, expressing the configurational contribution of a specific symmetry-equivalent figure to the formation energy of that configuration,

$$\bar{\Pi}_\alpha(\text{config}) = \frac{1}{ND_\alpha} \sum_{m=0}^{ND_\alpha} \hat{S}_1 \hat{S}_2 \cdots \hat{S}_{m_\alpha}, \tag{4.3}$$

with D_α as the number of figures of class α per site and N as the number of sites. $\bar{\Pi}_\alpha$ yields a value between -1 and $+1$. Equation (4.3) can now be rewritten as a function of symmetry-equivalent clusters α and correlation functions $\bar{\Pi}_\alpha$,

$$\Delta H^c_{CE}(\text{config}_k) = \sum_\alpha J_\alpha \sigma_\alpha = \sum_\alpha J_\alpha D_\alpha \bar{\Pi}_\alpha(\text{config}) \quad \text{for } k = 1 \text{ to } 6, \tag{4.4}$$

for the six CuPt compounds $A_{4-n}B_n$, with n=0,1,2,2,3,4. The $\bar{\Pi}_\alpha(\text{config}_k)$ of each symmetry-equivalent cluster α can easily be calculated for ordered fcc configurations. Rewritten in the vector-matrix notation, Eq. (4.4) results in a 6×6 matrix that expresses the relation between the interaction parameters J_α and the correction energies ΔH^c_{CE},

$$\begin{pmatrix} \Delta H^c_{CE}(\text{fccCu}) \\ \Delta H^c_{CE}(L1_2\text{Cu}_3\text{Pt}) \\ \Delta H^c_{CE}(L1_0\text{CuPt}) \\ \Delta H^c_{CE}(L1_2\text{CuPt}_3) \\ \Delta H^c_{CE}(\text{fccPt}) \\ \Delta H^c_{CE}(L1_1\text{CuPt}) \end{pmatrix} = \begin{pmatrix} 1 & 1 & 1 & 1 & 1 & 1 \\ 1 & 1/2 & 0 & -1/2 & -1 & 1 \\ 1 & 0 & -1/3 & 0 & 1 & 1 \\ 1 & -1/2 & 0 & 1/2 & -1 & 1 \\ 1 & -1 & 1 & -1 & 1 & 1 \\ 1 & 0 & 0 & 0 & -1 & -1 \end{pmatrix} \begin{pmatrix} J_0D_0 \\ J_1D_1 \\ J_2D_2 \\ J_3D_3 \\ J_4D_4 \\ J_5D_5 \end{pmatrix}. \tag{4.5}$$

A simple matrix inversion yields J_α,

$$\begin{pmatrix} J_0D_0 \\ J_1D_1 \\ J_2D_2 \\ J_3D_3 \\ J_4D_4 \\ J_5D_5 \end{pmatrix} = \begin{pmatrix} 0.0625 & 0.0 & 0.375 & 0.0 & 0.0625 & 0.5 \\ 0.25 & 0.5 & 0.0 & -0.5 & -0.25 & 0.0 \\ 0.375 & 0.0 & -0.75 & 0.0 & 0.375 & 0.0 \\ 0.25 & -0.5 & 0.0 & 0.5 & -0.25 & 0.0 \\ 0.0625 & -0.25 & 0.375 & -0.25 & 0.0625 & 0.0 \\ 0.0 & 0.25 & 0.0 & 0.25 & 0.0 & -0.5 \end{pmatrix} \begin{pmatrix} \Delta H^c_{CE}(\text{fccCu}) \\ \Delta H^c_{CE}(L1_2\text{Cu}_3\text{Pt}) \\ \Delta H^c_{CE}(L1_0\text{CuPt}) \\ \Delta H^c_{CE}(L1_2\text{CuPt}_3) \\ \Delta H^c_{CE}(\text{fccPt}) \\ \Delta H^c_{CE}(L1_1\text{CuPt}) \end{pmatrix}, \tag{4.6}$$

with $D_0=1$, $D_1=1$, $D_2=12$ (i.e., the number of the first NN), $D_3=24$, $D_4=8$, and $D_5=6$ (the number of the second NN).

After having determined all J_α parameters, the energy for every arbitrary configuration is evaluated as

$$\Delta H^f_{MEAM\text{-}CEM} = \Delta H^f_{MEAM} + \Delta H^c_{CEM}. \tag{4.7}$$

The volume-dependent heats of formation of the six ordered CuPt alloys are calculated with this scheme and can then be compared with volume-dependent MEAM and DFT-PW91 (VASP) energies. Figure 2 illustrates the ability of the original MEAM to correctly predict the lattice parameter and the bulk modulus of relaxed ordered alloys. However, Fig. 2 also reveals that the original MEAM fails to quantitatively predict the magnitude of the heat of formation. It thus makes sense to include a limited number of CEM parameters, only to correct the heat of formation of a number of relaxed ordered alloys. The additional CEM parameters do not influence the prediction of the lattice parameter or the bulk modulus.

Then, the energies of these structures and of a number of atomic slabs with single antisite defects are calculated with MEAM-CEM and compared with DFT-PW91 (QE) results. For the $L1_2$ structure, we have considered periodic slabs with six layers and 2×2 atoms per layer and slabs with four layers and 4×4 atoms per layer. For the $L1_1$ structure, periodic atomic slabs were considered with six 2×2 layers and with six 3×3 layers. These slabs were filled according to the $L1_2$ or $L1_1$ symmetry but with one Cu (Pt) atom replaced by a Pt (Cu) atom. Figure 3 illustrates the defect-free $L1_2$, $L1_1$, and $L1_0$ energies and the formation energies of periodic slabs that are based on these structures but with single Pt (Cu) antisite defects. The formation energy ΔH^f_{AS} of an isolated bulk antisite defect in a perfectly ordered stoichiometric atomic slab was calculated as follows:[29]

$$\Delta H^f_{AS} = \Delta H^f_{bulk}(N^A_{bulk}-1, N^B_{bulk}+1) - (N^A_{bulk}+N^B_{bulk})\Delta H^f_{bulk}, \tag{4.8}$$

where N^A_{bulk} (N^B_{bulk}) is the number of A (B) atoms in the bulk and ΔH^f_{bulk} ($N^A_{bulk}-1, N^B_{bulk}+1$) is the formation energy of an atomic slab that refers to the perfectly ordered bulk, but with one B excess atom on an A site. The larger model slabs are necessary for the calculation in order to consider isolated defects. Table II presents a comparison between MEAM, MEAM-CEM, and DFT-PW91 (QE) calculations of formation energies of pairs of antisite defects in stoichiometric ordered CuPt compounds.

The MEAM-CEM features a very satisfying agreement for the prediction of the heat of formation, the bulk modulus, the lattice parameter of relaxed ordered CuPt alloys, and the formation energy of bulk antisite defects. This is achieved by combining the ability of MEAM to accurately describe structural bulk deformations in metallic alloys with the versatility of CEM to include the ground state *ab initio* calculations of an arbitrary number of ordered alloys. It is therefore deemed a considerable improvement over the original MEAM. Moreover, the MEAM-CEM algorithm, elaborated in this paper, has a degree of complexity and parametrization effort that remains comparable to the original MEAM. The extension of MEAM with CEM in this work only induces a small number of additional interaction parameters, but it manifestly gives an added value in view of the closer agreement with the DFT-PW91 benchmarks.

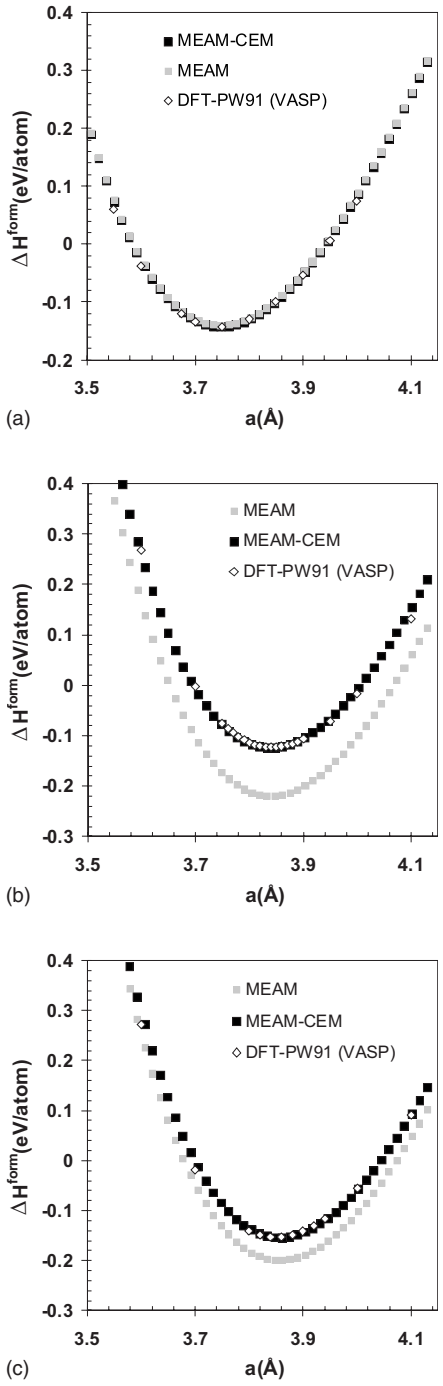

FIG. 2. [(a)–(c)] Volume-dependent heat of formation of $L1_2$ Cu_3Pt, $L1_0$ CuPt, and $L1_1$ CuPt, as calculated with DFT-PW91 (VASP) (◇), MEAM (gray square), and MEAM-CEM (■). (a) corresponds to the MEAM reference structure $L1_2$ Cu_3Pt; the MEAM heat of formation of $L1_0$ CuPt is—erroneously—more exothermic than $L1_1$ CuPt [gray □ in (b) and (c)]. The cluster expansion correction restores the stability of $L1_1$ CuPt, as compared to $L1_0$ CuPt, in agreement with DFT-PW91 (VASP).

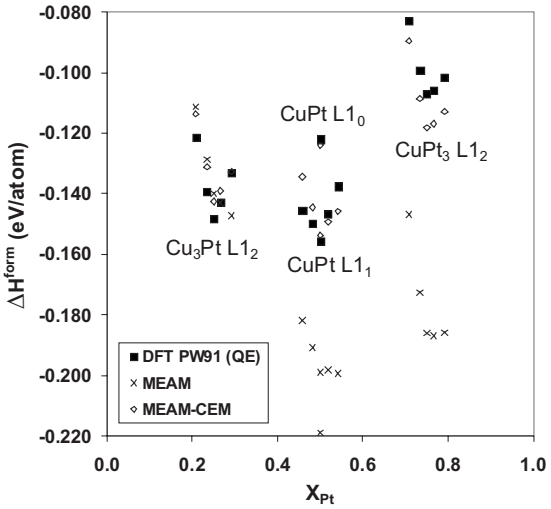

FIG. 3. MEAM, MEAM-CEM, and DFT-PW91 (QE) predictions for the heat of formation of various ordered CuPt compounds with Cu-rich and Pt-rich antisite defects.

Combining the MEAM-CEM with MC simulations allows us to gain information on the short- and long-range orders at equilibrium. Therefore, to confirm the stability of the ordered alloys predicted with MEAM-CEM, the ground state accuracy is tested in a final step by calculating the order-disorder transition temperatures T_C of $L1_2$ Cu_3Pt, $L1_1$ CuPt, and $L1_2$ $CuPt_3$ in a series of MC simulations. In order to determine the order-disorder T_C from MC simulations, virtual crystals are constructed with $24\times24\times24$ lattice sites. Simulations are performed with the Metropolis algorithm,[33] starting with crystals in the ordered state. After 30×10^6 Markov steps, equilibrium can safely be assumed, and from there on, the heat of formation ΔH^f of the simulated crystal, the short-range order (SRO),[34] and the long-range order parameters are sampled every 25 000 additional steps and averaged over another 10×10^6 steps. In order to evaluate the critical order-disorder temperature T_C, a succession of simulations is performed at gradually increasing temperatures (in steps of 50 K). At T_C, the long-range order parameter rather abruptly drops from a value close to 1 to nearly zero. This procedure is performed both with MEAM and MEAM-CEM, and their predictions of T_C are compared with experimental values[25] in Table III. At the three canonical compositions, the MEAM-CEM simulations of CuPt alloys now correspond to the experimentally determined ground states.

TABLE II. Formation energy of pairs of isolated antisite defects in stoichiometrically ordered CuPt compounds.

	Antisite defect energies (eV/antisite)	
Structure	DFT-PW91 (QE)	MEAM-CEM
Cu_3Pt $L1_2$	0.912	0.963
CuPt $L1_1$	0.794	0.730
$CuPt_3$ $L1_2$	0.589	0.692

TABLE III. MEAM and MEAM-CEM predictions of the critical temperature T_C of order-disorder transitions for three CuPt compounds. For the equiatomic CuPt alloy, MEAM predicts an $L1_0$ order; the corresponding T_C is listed for comparison.

	T_C (K)		
	MEAM-CEM	MEAM	Expt.[23]
Cu_3Pt $L1_2$	1225	725	870
CuPt $L1_1$	875 ($L1_1$)	625 ($L1_0$)	1089 ($L1_1$)
$CuPt_3$ $L1_2$	950	1025	850

V. MODIFIED EMBEDDED ATOM METHOD–CLUSTER EXPANSION METHOD DESCRIPTION OF CuPt SURFACES

A. Surface energy of fcc Cu and fcc Pt with modified embedded atom method–cluster expansion method

By construction, the MEAM-CEM prediction for the heat of formation for the bulk materials Cu, Pt, and $L1_2$ Cu_3Pt coincides exactly with the *ab initio* value. In the case of anisotropic defects, however, a number of figures with interaction energy J_α drop out of the MEAM-CEM calculation, and the remaining CEM term no longer vanishes entirely. However, the MEAM parameters are determined in a least-squares fitting scheme to, among other quantities, the pure-element unrelaxed (111) and (100) surface energies. Consequently, CEM parameters disturb the least-squares precision of MEAM for these quantities. A good MEAM description that keeps a CEM correction small is therefore crucial for accurate MEAM-CEM total energy predictions.

An important step in the further validation of the CEM parameters is now to recalculate the pure-element Cu and Pt surface energies of low index orientations with MEAM-CEM and to compare them with MEAM and DFT-PW91 (VASP) results. Provided a lattice film is considered with a sufficient number of atomic layers to eliminate the influence of the surface in the core layers and with periodic boundary conditions in two directions perpendicular to the surface, the surface energy ΔH^{surf} per atom in a pure-element lattice can be calculated as

$$\Delta H^{surf}(k) = \frac{\Delta H^{film}(k,N) - N\Delta H^f_{bulk}}{N^{surf}a^{surf}}. \qquad (5.1)$$

In this expression, $\Delta H^{film}(k,N)$ is the formation energy of a metallic film with two surfaces in direction k and N represents the total number of atoms in the film. $N\Delta H^f_{bulk}$ is the formation energy of a bulk metal with N atoms and N^{surf} denotes the number of surface atoms in the film, with a^{surf} as the surface area per atom of the film. In pure materials, ΔH^f_{bulk} equals ΔH^{sub}, with ΔH^{sub} as the sublimation energy per atom of the (fully relaxed) bulk material.

Table IV compares the DFT-PW91 (VASP), MEAM-CEM, and MEAM surface energies of the pure-element fcc Pt and Cu low index surfaces. The DFT-PW91 surface energies were found to have converged with respect to the number of

TABLE IV. MEAM-CEM, MEAM, and DFT-PW91 (VASP) predictions of the unrelaxed surface energy of fcc Cu and fcc Pt at three low index surfaces.

	Cu			Pt		
	MEAM-CEM	MEAM	DFT-PW91 (VASP)	MEAM-CEM	MEAM	DFT-PW91 (VASP)
$\gamma_{(100)}$ (eV/Å^2)	0.087	0.092	0.091	0.123	0.118	0.114
$\gamma_{(111)}$ (eV/Å^2)	0.074	0.080	0.080	0.094	0.091	0.092
$\gamma_{(110)}$ (eV/Å^2)	0.092	0.096	0.097	0.120	0.115	0.121

film layers as a variation between 7, 9, and 11 layers did not result in significant variations of the surface energy. In view of the deviation tolerated for the (110) surface energy, which is part of the MEAM test set, the loss of accuracy of MEAM-CEM was not considered significant enough to start a reiteration of the MEAM and CEM parametrization and to create a closed loop between steps 3 and 1 mentioned in Fig. 1. If the perturbation of the surface energies would be significant, one could either choose a global, simultaneous optimization of the MEAM and the CEM parameters or a correction of the surface interactions through the definition of layer-dependent cluster interactions. Because MEAM describes extended defects with a good accuracy and CEM only restores the stability of the $L1_1$ ground state, no reiteration of this kind was deemed necessary in this work. We will verify this assumption through the calculation of a test set of alloy surface and segregation energies.

B. Surface energy of CuPt alloys

At $T \ll T_C$, the equilibrium surface composition of ordered metallic alloys generally corresponds to a bulk-terminated surface. Ordered alloys display an oscillating bulk composition profile in the (100) and (110) directions of $L1_2$, in the (100) direction of $L1_0$, and in the (111) direction of $L1_1$. At least two distinct surface terminations are then possible. The stability of each possible termination can be described by the surface energy. Starting from free atoms in the gas phase, the surface energy $\Delta H^{surf}(k)$ of an alloy film amounts to[29]

$$\Delta H^{surf}(k) = \frac{\Delta H^{film}(k, N^A_{film}, N^B_{film}) - N^A_{film}\Delta H^{sub}(A) - N^B_{film}\Delta H^{sub}(B) - (N^A_{film} + N^B_{film})\Delta H^f_{bulk}}{N^{surf} a^{surf}}, \tag{5.2}$$

with N^A_{film} (N^B_{film}) as the number of atoms of each atomic species A (B) in the atomic film and with ΔH^f as the total heat of formation of the bulk alloy. Surfaces of ordered alloys with an oscillating bulk profile can have surface terminations with totally different atomic compositions. First, the different surface energies are calculated with MEAM-CEM according to Eq. (5.2) for the surfaces for which the segregation is simulated in Sec. V C. The results, presented in the three leftmost columns of Table V, give a suggestion to identify the relative stability of unreconstructed surface terminations in the ordered CuPt alloys with an oscillating bulk composition profile. These results will help us to discuss segregation and the stability of the different possible surface structures in CuPt. However, the expression of the surface energy as given in Eq. (5.2) is not yet complete. Whenever the stoichiometry of a slab used to compute the surface energy differs from that of the bulk, the energy of this difference has to be accounted for by the chemical potential μ of the excess species,[35,36]

$$\Delta H^{surf}(k) = \frac{1}{N^{surf} a^{surf}} \Bigg(\Delta H^{film}(k, N^A_{film}, N^B_{film}) - N^A_{film}\Delta H^{sub}(A) - N^B_{film} \times \Delta H^{sub}(B) - (N^A_{film} + N^B_{film})\Delta H^f_{bulk} - \mu \sum_{i=1}^{SL} (c_i - c) \Bigg), \tag{5.3}$$

with SL as the number of layers in the surface region, $\{c_i\}$ the concentration profile of some finite surface region, and c the concentration in the bulk. The chemical potential is not fixed but can always vary within a given range depending on the identity of the excess atoms in the bulk. This makes computed surface energies according to Eq. (5.3) not readily interpretable to the stability of surface terminations. We therefore also calculated segregation energies from bulk Cu and Pt antisite defects,[29]

TABLE V. A selection of MEAM-CEM, DFT-LDA (QE), and DFT-PW91 (QE) energies of unreconstructed surface terminations of CuPt compounds [following Eq. (5.2)]. Overall, the MEAM-CEM and the DFT calculations perform equally well in the identification of stable surface terminations.

	$\Delta H^{surf}_{(100)}$ (eV/Å^2) $L1_2$ Cu_3Pt								
	MEAM-CEM			DFT-LDA (QE)			DFT-PW91 (QE)		
Termination	Cu	CuPt	Pt	Cu	CuPt	Pt	Cu	CuPt	Pt
9 layers	0.100	0.109		0.133	0.133		0.104	0.098	
1 layer relaxed	0.098	0.109		0.132	0.133		0.103	0.098	
2 layer relaxed	0.098	0.109		0.132	0.133		0.103	0.097	
11 layers	0.100	0.109		0.133	0.134		0.104	0.098	
Termination	$\Delta H^{surf}_{(110)}$ (eV/Å^2) $L1_2$ Cu_3Pt								
	MEAM-CEM			DFT-LDA (QE)			DFT-PW91 (QE)		
	Cu	CuPt	Pt	Cu	CuPt	Pt	Cu	CuPt	Pt
9 layers	0.104	0.115		0.134	0.146		0.104	0.109	
1 layer relaxed	0.099	0.112		0.129	0.143		0.099	0.107	
2 layer relaxed	0.098	0.111		0.128	0.143		0.099	0.106	
11 layers	0.104	0.115		0.134	0.146		0.104	0.109	
Termination	$\Delta H^{surf}_{(111)}$ (eV/Å^2) $L1_1$ CuPt								
	MEAM-CEM			DFT-LDA (QE)			DFT-PW91 (QE)		
	Cu	CuPt	Pt	Cu	CuPt	Pt	Cu	CuPt	Pt
9 layers	0.101	0.092	0.069	0.140		0.100	0.113	0.105	0.072
1 layer relaxed	0.099	0.092	0.068	0.140		0.100	0.113	0.102	0.071
2 layer relaxed	0.099	0.092	0.068	0.140		0.100	0.113	0.102	0.071
11 layers	0.101	0.092	0.069	0.140		0.100	0.113	0.104	0.071
Termination	$\Delta H^{surf}_{(100)}$ (eV/Å^2) $L1_0$ CuPt								
	MEAM-CEM			DFT-LDA (QE)			DFT-PW91 (QE)		
	Cu	CuPt	Pt	Cu	CuPt	Pt	Cu	CuPt	Pt
9 layers	0.104	0.110	0.107	0.147		0.144	0.102	0.105	0.113
1 layer relaxed	0.100	0.110	0.107	0.147		0.143	0.099	0.104	0.113
2 layer relaxed	0.100	0.110	0.107	0.147		0.143	0.099	0.104	0.113
11 layers	0.104	0.110	0.107	0.147		0.144	0.101	0.105	0.113
Termination	$\Delta H^{surf}_{(100)}$ (eV/Å^2) $L1_2$ $CuPt_3$								
	MEAM-CEM			DFT-LDA (QE)			DFT-PW91 (QE)		
	Cu	CuPt	Pt	Cu	CuPt	Pt	Cu	CuPt	Pt
9 layers		0.120	0.115		0.149	0.145		0.113	0.109
1 layer relaxed		0.118	0.115		0.148	0.144		0.112	0.108
2 layer relaxed		0.118	0.115		0.148	0.144		0.112	0.108
11 layers		0.120	0.115		0.149	0.145		0.113	0.108
Termination	$\Delta H^{surf}_{(110)}$ (eV/Å^2) $L1_2$ $CuPt_3$								
	MEAM-CEM			DFT-LDA (QE)			DFT-PW91 (QE)		
	Cu	CuPt	Pt	Cu	CuPt	Pt	Cu	CuPt	Pt

TABLE V. (*Continued.*)

	$\Delta H^{surf}_{(100)}$ (eV/Å^2) $L1_2$ Cu_3Pt								
	MEAM-CEM			DFT-LDA (QE)			DFT-PW91 (QE)		
Termination	Cu	CuPt	Pt	Cu	CuPt	Pt	Cu	CuPt	Pt
9 layers		0.114	0.124		0.141	0.160		0.108	0.121
1 layer relaxed		0.108	0.121		0.135	0.156		0.102	0.118
2 layer relaxed		0.106	0.119		0.134	0.155		0.101	0.117
11 layers		0.114	0.124		0.141	0.161		0.107	0.121

$$\Delta H^{seg} = \frac{\Delta H^{film}(k, N^A_{film} - 2, N^B_{film} + 2)}{2} - \frac{\Delta H^{film}(k, N^A_{film}, N^B_{film})}{2} + (N^A_{bulk} + N^B_{bulk})\Delta H^f_{bulk} - \Delta H^f_{bulk}(N^A_{bulk} - 1, N^B_{bulk} + 1). \tag{5.4}$$

The individual terms in Eq. (5.4) are self-explanatory. For the calculation of segregation energies, atomically ordered films in a rigid lattice with a thickness of nine atomic layers with 2×2 atoms per layer are used. The lattice parameter is set equal to the fully relaxed bulk lattice parameter of the compound under consideration. The (100) and (110) surfaces of the $L1_2$ Cu_3Pt ($CuPt_3$) alloys are considered, both with a pure Cu (Pt) and an equiatomic CuPt (CuPt) bulklike termination, as are the (111) surface of the $L1_1$ CuPt with a pure Cu and a pure Pt bulklike termination. The same calculation is then repeated with an atomic antisite in each top layer of the film. Finally, the bulk antisite defect energy of isolated excess atoms is subtracted [Eq. (4.8)].

Before formulating a full assessment of the stability of CuPt low index surfaces based on surface energies, segregation energies, MC simulations, and the driving forces of surface segregation, the results of the surface and segregation energy calculations are first compared with a number of independent DFT calculations performed with the QE code.

The surface energies at different terminations for three canonical compositions, Cu_3Pt, CuPt, and $CuPt_3$, were computed within the framework of spin-restricted DFT using the QE package.[23] Using each of the fully relaxed Cu_3Pt ($L1_2$), CuPt ($L1_0$), CuPt ($L1_1$), and $CuPt_3$ ($L1_2$) unit structures as a basis, we have built supercells in the direction perpendicular to the surface of interest. This can also be viewed as creating a stack of layers parallel to the surface plane. By separating this stack from its periodic images with empty space, a suitable model was created for a film with a specific termination within three-dimensional periodic boundary conditions. From the energy of this slab, combined with the equilibrium energy per atom of Cu (fcc) and Pt (fcc), we can calculate the formation energy of an alloy film ΔH^{film} (n_i+n_j). Finally, from Eq. (5.2), we obtain the surface energy ΔH^{surf}. The DFT-LDA (QE) and DFT-PW91 (QE) surface energies at different terminations are presented in the middle and right columns of Table V for three canonical compositions, Cu_3Pt, CuPt, and $CuPt_3$.

The convergence of the surface energy with respect to the number of layers in the film and the size of the vacuum in the supercell has been ascertained. It turns out that a vacuum separation of 15 a.u. plus one lattice constant perpendicular to the surface under investigation is largely sufficient to achieve reasonable convergence. The convergent behavior of the surface energy at various film thicknesses is reflected in Table V, where the values are tabulated corresponding to 9 and 11 layers. Also included in Table V are the resulting surface energies where, respectively, one and two layers at both sides of the film were relaxed.

In summary, we would like to stress the good qualitative agreement of the three methods for all terminations and compositions, except for the (100) layer in $L1_2$ Cu_3Pt, for which the DFT-PW91 (QE) method finds a lower surface energy, different from both the DFT-LDA (QE) and the MEAM-CEM method. Quantitatively, we observe that the DFT-LDA (QE) method tends to overestimate the surface energies in comparison with the DFT-PW91 (QE) method. If we consider the difference originating from the use of different functionals as a measure of the error that can be expected in DFT predictions of surface energies, it becomes clear just how close the MEAM-CEM energies coincide with the DFT-PW91 (QE) energies. This is a comforting result: The MEAM-CEM method closely reproduces results from the same DFT functional on which the MEAM-CEM method was initially parametrized, even with another program package.

Table VI presents a comparison between MEAM-CEM and DFT-PW91 (QE) calculations of surface [Eq. (5.2)] and segregation energies [Eq. (5.4)] of antisite defects. For CuPt and $CuPt_3$, we notice a reasonable agreement. It should be stressed that the computational load for the evaluation of segregation energies is heavy. The agreement is less good for Cu_3Pt and this conclusion holds for both surface and segregation energies. Because the surface energies are in reasonably good agreement and because, by definition, the segregation energy describes only the segregating atom in one particular ordered environment,[29] it probably fails to quantitatively describe the segregation profile of (partly) disordered alloys at finite temperatures. It then follows that for alloy surfaces, SRO must be taken into account, which demands a large number of atoms per layer to be considered. This is done in the remaining part of this work, where we focus on surface MC simulations and compare them with experimental results. The segregation energies of Table VI and the differences between MEAM-CEM and DFT-PW91 (QE) will be considered in the interpretation of the MEAM-CEM/MC surface segregation profiles.

TABLE VI. Surface energies of stoichiometrically ordered CuPt compounds with different surface terminations. Bulk terminations are considered with single antisite defects at the surface. In the atomic film, consisting of nine layers and 2×2 atoms per layer, one antisite defect in each surface layer is constructed in order to conserve the symmetry of the atomic slab. Each slab is relaxed according to the equilibrium bulk lattice parameter (Table I).

				Surface energy (eV/atom)		Segregation energy (eV/atom)	
Structure	Surface orientation	Initial termination	Segregating species	DFT-PW91 (QE)	MEAM-CEM	DFT-PW91 (QE)	MEAM-CEM
Cu_3Pt $L1_2$	(100)	CuPt	Cu	0.788	0.838	−0.183	−0.421
	(100)	CuPt	Pt	0.752	0.801	−0.094	−0.062
	(100)	Cu	Pt	0.765	0.768	−0.220	0.042
Cu_3Pt $L1_2$	(110)	CuPt	Cu	1.168	1.169	−0.242	−0.595
	(110)	CuPt	Pt	1.203	1.148	−0.092	0.051
	(110)	Cu	Pt	1.074	1.067	−0.198	−0.045
CuPt $L1_1$	(111)	Cu	Pt	0.754	0.682	−0.407	−0.145
	(111)	Pt	Cu	0.526	0.565	−0.086	−0.028
$CuPt_3$ $L1_2$	(100)	Pt	Cu	0.864	0.889	−0.042	−0.036
	(100)	CuPt	Cu	0.868	0.888	−0.169	−0.203
	(100)	CuPt	Pt	0.962	1.046	−0.221	−0.100
$CuPt_3$ $L1_2$	(110)	Pt	Cu	1.289	1.300	−0.269	−0.222
	(110)	CuPt	Cu	1.173	1.209	−0.170	−0.158
	(110)	CuPt	Pt	1.324	1.310	0.006	−0.282

C. Monte Carlo simulations of surface segregation in CuPt alloys

We have performed canonical MEAM-CEM/MC calculations to investigate the segregation to the three low index surfaces of CuPt, at three stoichiometric "canonical" compositions and at temperatures between 300 and 1900 K. The off-stoichiometric effect was also considered by performing MC simulations with limited excess Cu-rich and excess Pt-rich deviations of the stoichiometric compositions so that, at equilibrium, only a slight ($<\pm1.0\%$) deviation of the bulk stoichiometric composition exists. In this way, the discontinuity of the chemical potential [Eq. (5.3)] at the stoichiometric composition is taken into account.[36,37] The simulations allow for a full discussion on the temperature- and composition-dependent multilayer segregation in CuPt alloys based on one energy model with 10 pure-element and 11 alloy parameters. Exactly the same set of parameters is used to investigate all the considered compositions, surface orientations, and temperatures below and above T_C, illustrating the transferability of these MEAM-CEM parameters. Simulations were performed in the Metropolis algorithm[33] with a simulation slab of 35 atomic layers and 24×24 atoms in each layer. If the segregation of bulk atoms to the surface region has an influence on the bulk concentration in an atomic slab, well below the surface region, a new simulation is started with an additional excess of the segregating species in order to keep the bulk concentration constant with respect to the concentration under study.

1. $L1_2$ Cu_3Pt

The bulk of $L1_2$ Cu_3Pt features oscillating profiles in the (110) and the (100) direction with two possible surface terminations. Surface composition profiles of the $Cu_{3\pm\delta}Pt_{1\mp\delta}$ alloys, obtained from MEAM-CEM/MC simulations, are presented in Fig. 4. Stable and metastable terminations are first considered by initiating the simulations with a Cu-rich and an equiatomic termination. MEAM-CEM/MC simulations find for all $Cu_{3\pm\delta}Pt_{1\mp\delta}$ (100) and (110) surfaces that the lower surface energy of Cu in comparison with Pt (Table VI) is the major factor determining the surface termination and segregation. This results in a pure Cu termination at the (110) and (100) surfaces of the $Cu_{3\pm\delta}Pt_{1\mp\delta}$ alloys at $T<T_C$. The equiatomic CuPt termination is found to be metastable only in Pt-rich $Cu_{3-\delta}Pt_{1+\delta}$ at very low temperatures (<500 K). Above T_C, the atomic layers of the bulk alloy become random and stoichiometric. The surface layer then remains largely enriched with Cu, and the subsurface layers show an oscillating segregation profile damping out to the bulk composition. This profile is typical for disordered alloys with attractive interatomic *AB* interactions. The oscillations in the segregation profile become attenuated as T increases further above T_C. In stoichiometric $L1_2$ Cu_3Pt and at $T\ll T_C$, MEAM-CEM predicts an ordered (111) surface with the stoichiometric composition. As T approaches T_C, the increased entropy and the lower surface energy of Cu yield a Cu enrichment (to 77.5%), which is almost entirely confined to the very surface layer. The Cu enrichment again gradually di-

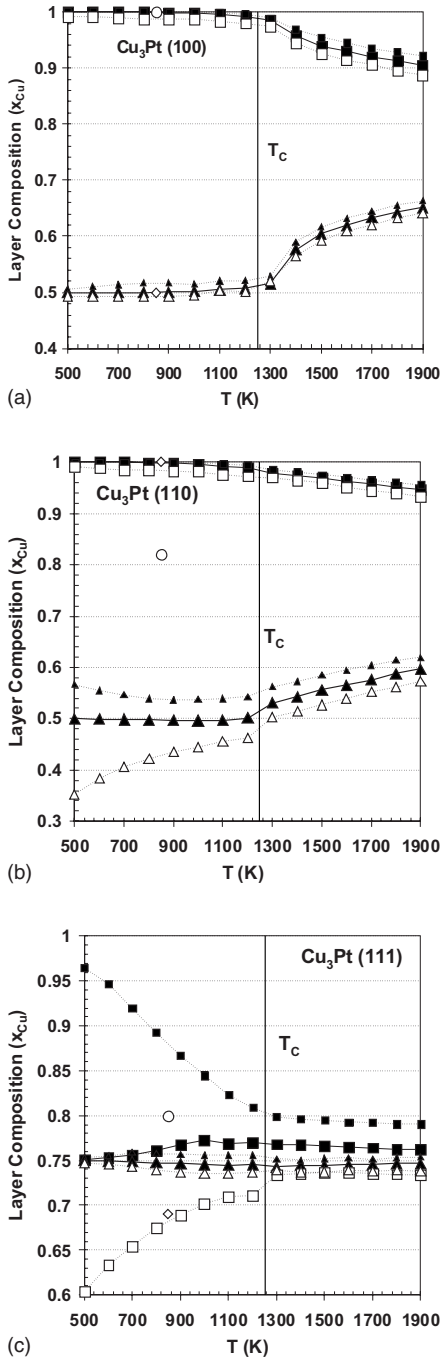

FIG. 4. [(a)–(c)] Composition of the surface (■, ■, □) and subsurface (▲, ▲, △) layers of the low index surfaces in the stoichiometric Cu_3Pt (■, ▲), the Cu-rich $Cu_{3+\delta}Pt_{1-\delta}$ (■, ▲), and the Pt-rich $Cu_{3-\delta}Pt_{1+\delta}$ (□, △) alloys versus temperature. LEIS measurements of the surface (○) and subsurface (◇) composition of Cu_3Pt (100) (Ref. 47), (110) (Ref. 46), and (111) (Refs. 48 and 49) were added to compare the segregation profiles with available experimental evidence.

minishes to the stoichiometric bulk composition when T increases further above T_C. The off-stoichiometric effect leads to a pronounced exothermic Cu (Pt) segregation in $Cu_{3+\delta}Pt_{1-\delta}$ ($Cu_{3-\delta}Pt_{1+\delta}$) that gradually diminishes at increasing temperatures and eventually evolves to the bulk composition far above T_C.

2. $L1_1$ *CuPt*

In the equiatomic $L1_1$ CuPt alloy, the layer-by-layer bulk composition profiles in the (110) and the (100) direction are stoichiometric. Figure 5 presents the temperature-dependent surface and subsurface concentrations of the equiatomic $Cu_{1\pm\delta}Pt_{1\mp\delta}$ alloys predicted with MEAM-CEM/MC simulations. Well below T_C, the simulations predict a Cu-rich (110) and a somewhat less Cu-rich (100) surface. Over a few layers, the oscillations in the subsurface composition gradually fade to the bulk stoichiometric composition. With an excess Cu concentration in the bulk, both (110) and (100) surfaces become fully enriched with Cu, while with an excess Pt concentration in the bulk, both surfaces have a surface layer with 50% Cu. When T increases to T_C, the Cu concentration in the surfaces of the stoichiometric and the Pt-rich simulation slabs also increases and enhances the subsurface oscillations. In these slabs, the Cu surface concentration reaches a maximum in the neighborhood of T_C, at 800 K, with a (110) [(100)] surface composition varying from 71% (80%) Cu in atomic slabs with excess Pt to 84% (90%) in stoichiometric equiatomic slabs. At temperatures increasing above T_C, the oscillations diminish and the surface concentration evolves to the bulk concentration.

The (111) surface of the ordered $L1_1$ alloy evolves to a pure Pt termination in stoichiometric, Pt-rich, and Cu-rich $Cu_{1\pm\delta}Pt_{1\mp\delta}$ samples below T_C. A metastable Cu (111) surface termination was found at low temperatures only if the simulation was initiated with an atomic slab with a Cu surface. At $T > T_C$, Pt segregates to the surface on top of an oscillating subsurface region. The face-dependent surface composition at the different low index surfaces of the equiatomic CuPt is one of the more striking results of this study. A comparison between MEAM-CEM/MC surface simulations and the DFT and MEAM-CEM calculations in Tables V and VI reveals an excellent agreement supporting the face-dependent segregation in equiatomic CuPt.

3. $L1_2$ $CuPt_3$

MEAM-CEM/MC simulations predict that the strain release of Pt atoms with the larger atomic radius and the ordering effect of the majority Pt atoms at the surface of $Cu_{1\pm\delta}Pt_{3\mp\delta}$ promotes a Pt-rich termination of the (100) surface (Fig. 6). Below T_C, this results in a stable pure Pt termination of the ordered alloy. The (100) surface is also enriched with Pt above T_C, and the subsurface layers oscillate to the stoichiometric composition. The off-stoichiometric Cu-rich $Cu_{1+\delta}Pt_{3-\delta}$ alloy has a metastable equiatomic (100) termination at very low temperature (<600 K). At the (110) surface, the difference between the surface energy of Cu and Pt atoms is larger. The balance of the driving forces for surface segregation then shifts to a Cu-rich termination. Energetically, the (110) surface favors a mixed termination with 50% Pt. However, at the (110) surface, a Pt termination is metastable in the Pt-rich $Cu_{1-\delta}Pt_{3+\delta}$ alloy (<600 K). The Cu concentration in the surface evolves to the bulk composition as T approaches T_C.

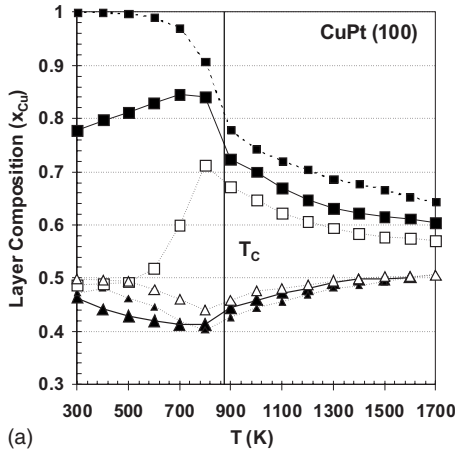

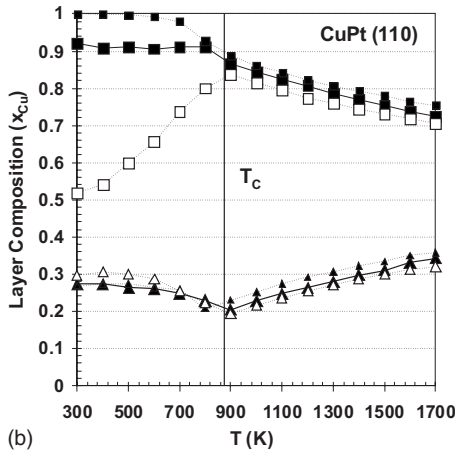

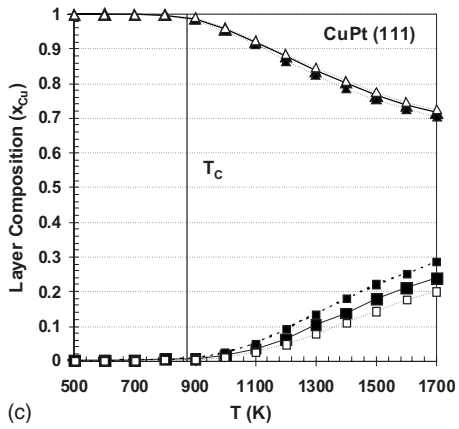

FIG. 5. [(a)–(c)] Composition of the surface (■, ■, □) and subsurface (▲, ▲, △) layers of the low index surfaces in the stoichiometric CuPt (■, ▲), the Cu-rich $Cu_{1+\delta}Pt_{1-\delta}$ (■, ▲), and the Pt-rich $Cu_{1-\delta}Pt_{1+\delta}$ (□, △) alloys versus temperature.

$L1_2$ $CuPt_3$ features stoichiometric layers in the (111) direction of the bulk alloy. Hence, only a small influence of surface segregation would be expected in the stoichiometric alloy. However, a pure Pt (111) surface with a sandwichlike subsurface rearrangement is formed with very pronounced oscillations up to the fourth layer (Fig. 7). A similar profile is found at the (111) surfaces of Cu- and Pt-enriched $L1_2$

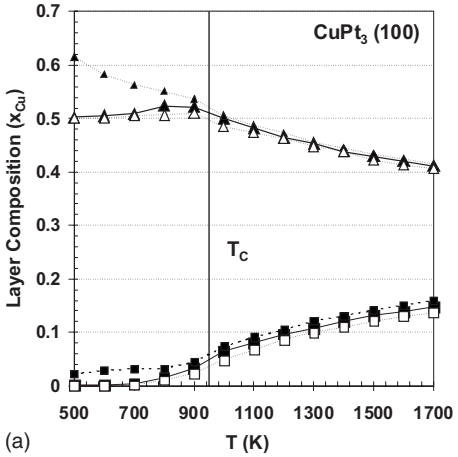

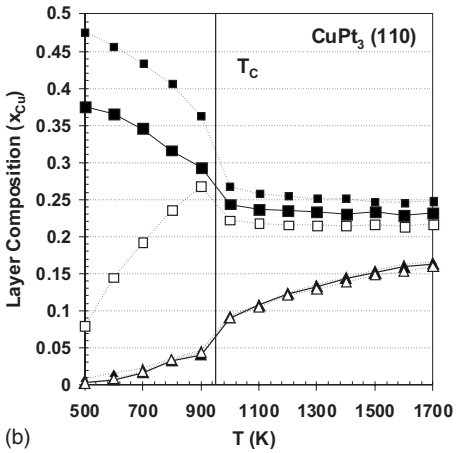

FIG. 6. [(a) and (b)] Composition of the surface (■, ■, □) and subsurface (▲, ▲, △) layers of the low index surfaces in the stoichiometric $CuPt_3$ (■, ▲), the Cu-rich $Cu_{1+\delta}Pt_{3-\delta}$ (■, ▲), and the Pt-rich $Cu_{1-\delta}Pt_{3+\delta}$ (□, △) alloys versus temperature.

$CuPt_3$. At $T > T_C$, the composition oscillates up to the eighth layer and attenuates as T rises further.

VI. DISCUSSION

A. Driving forces for surface segregation in CuPt

In this section, the driving forces for surface segregation in CuPt alloys are first discussed in more detail. Subsequently, in Sec. VI B, the surface terminations and segregation profiles calculated with MEAM-CEM and DFT will be discussed with reference to published experimental and theoretical evidence on surface structures in CuPt.

In the absence of a reactive gaseous atmosphere, three driving forces for segregation have been distinguished:[38,39] the lowering of the surface energy, the lowering of the mixing energy, and the (partial) release of elastic strain energy. Table VII gives an overview of experimental values of the Cu and Pt material properties that are related to these driving forces. The higher ΔH^{sub} of Pt leads to a higher surface energy of Pt as compared to Cu. At alloy surfaces, the atoms occupy surface areas that, ignoring relaxation effects, are

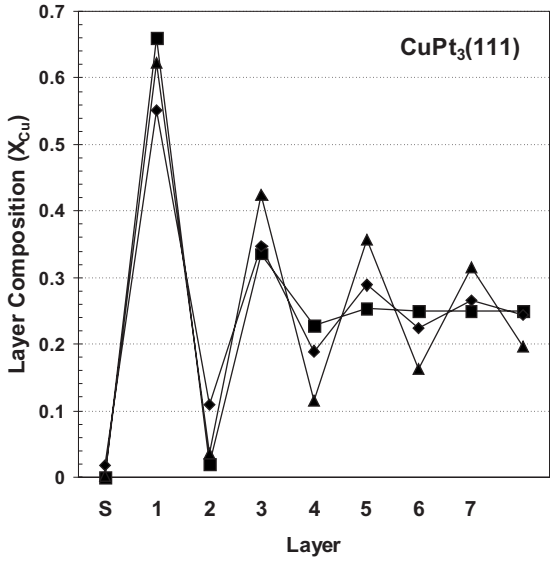

FIG. 7. Surface segregation profiles of stoichiometric $CuPt_3$ at the (111) surface in the ordered state at $T=500$ K (■) and at 1000 K (▲) and in the disordered state at $T=1500$ K (◆) ($T_C^{MEAM\text{-}CEM}=950$ K).

equally large. The surface energy per atom is then more closely related to the driving force for surface segregation than surface energy per unit area. Consequently, the surface energy is a more prominent driving force for segregation at more open surfaces.[45] This is illustrated by Table VIII for the CuPt system. The preference for Cu-rich surfaces at (110) orientations of the CuPt alloys is now easily understood in view of the larger difference in surface energy between Cu and Pt atoms at the (110) surface. From the surface composition profiles in Sec. V C, it appears that a more subtle interplay between elastic strain release and the less pronounced effect of surface energy at the other surface orientations can shift Cu segregation to Pt segregation.

Figure 8 plots the MEAM-CEM (100) surface energies per atom of pure Cu and pure Pt as a function of bulk interatomic distance R. The steep curve of pure Pt arises from strain energy that builds up in the bulk and is relieved at the surface. The surface energies per atom of Cu_3Pt and $CuPt_3$ are plotted in Fig. 9 and illustrate that strain release is more important in the latter. This figure supports the idea that strain release is a driving force for the segregation of the larger Pt atoms in $CuPt_3$ and that it is negligible in Cu_3Pt.

TABLE VII. Experimental values of Cu and Pt pure-element properties related to the driving forces for surface segregation. The surface energies in Refs. 43 and 44 correspond to surface free energies calculated from liquid surface tension parameters at the melting temperatures.

	Pt	Cu
Crystal structure	fcc	fcc
Lattice parameter (Å)	3.9158[a]	3.6075[a]
	3.9240[b]	3.6147[b]
Atomic radius (Å)	1.38[b]	1.248[b]
Heat of sublimation (eV/atom)	5.86[c]	3.50[c]
Surface energy (eV/Å^2)	0.138[d]	0.098[d]
	0.155[e]	0.114[e]

[a]Reference 40.
[b]Reference 41.
[c]Reference 42.
[d]Reference 43.
[e]Reference 44.

The exothermic mixing energy influences the surface segregation in order to maximize the number of bonds between unlike atomic species. In stoichiometric ordered alloys, this mechanism results in the segregation of the majority component to the surface region. In off-stoichiometric ordered alloys, the segregation of excess atoms is enhanced.

Finally, in stoichiometric systems with exothermic mixing energy, segregation at temperatures below T_C can depend on a combination of bulk entropy (endothermic segregation) and segregation enthalpy (exothermic contribution). In stoichiometric *ordered* systems, the enrichment of the surface can be seen as a two-step process. First, in an endothermic step, a bulk antisite defect is created in the ordered system. In the next step, one of the antisite atoms, generally the one with the lower surface energy, moves from the antisite in the bulk to form an antisite at the surface. In order to provide a driving force for segregation, this second step is exothermic. In equilibrium segregation to surfaces of stoichiometrically ordered systems, the balance between these two steps determines which species segregates and the amount of segregation, which on the whole may be endothermic (e.g.,

TABLE VIII. MEAM-CEM, MEAM, and DFT-PW91 (VASP) predictions of the unrelaxed surface energy *per atom* of fcc Cu and fcc Pt at three low index surfaces. At alloy surfaces, the different atoms occupy equal areas. The surface energy per atom is then more closely related to the driving force for surface segregation than surface energy per unit area (Table IV). This table illustrates that, in CuPt, surface energy is a more prominent driving force for surface segregation at more open surfaces.

	Cu			Pt		
	MEAM-CEM	MEAM	DFT-PW91 (VASP)	MEAM-CEM	MEAM	DFT-PW91 (VASP)
$\gamma_{(100)}$ (eV/atom)	0.580	0.612	0.606	0.978	0.938	0.907
$\gamma_{(111)}$ (eV/atom)	0.426	0.461	0.461	0.654	0.627	0.634
$\gamma_{(110)}$ (eV/atom)	0.866	0.904	0.913	1.350	1.293	1.361

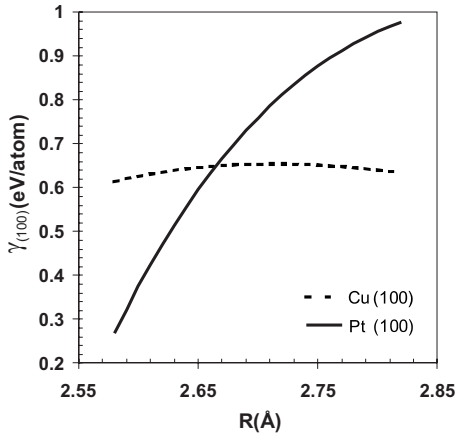

FIG. 8. MEAM-CEM (100) surface energy per atom of pure Cu (--) and pure Pt (—) as a function of bulk interatomic distance R. In this figure, R ranges from the DFT-PW91 (VASP) equilibrium interatomic distance in pure fcc Cu (2.58 Å) to pure fcc Pt (2.82 Å).

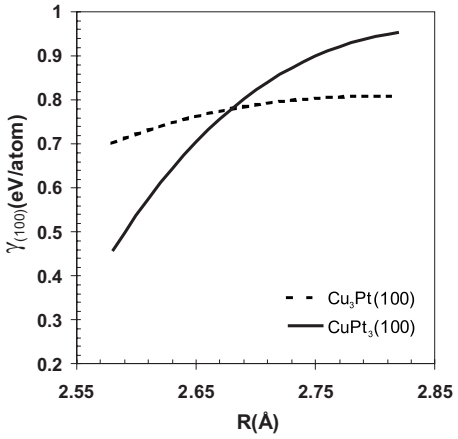

FIG. 9. MEAM-CEM (100) surface energy per atom of CuPt-terminated $L1_2$ Cu_3Pt (--) and CuPt-terminated $L1_2$ $CuPt_3$ (—) as a function of bulk interatomic distance R. In this figure, R ranges from the DFT-PW91 (VASP) equilibrium interatomic distance in pure fcc Cu (2.58 Å) to pure fcc Pt (2.82 Å).

exothermic bulk heat of formation, small difference in surface energy) or exothermic (e.g., small exothermic bulk heat of formation, large difference in surface energy). In systems with endothermic segregation, the amount of segregation is thus governed by the entropy-driven creation of bulk antisite defects. In these systems, two different segregation regimes can be recognized in function of temperature, since in disordered systems at $T > T_C$ segregation is always exothermic. The amount of segregation then reaches a maximum value in the neighborhood of T_C.

Endothermic, entropy-driven segregation can also occur in an *off-stoichiometric ordered* system if the segregation energy of the excess element is less exothermic than the segregation energy of the other element. In that case, segregation of the other element increases with temperature as the number of antisites of the other element grows.

B. Surface segregation in CuPt alloys

1. $L1_2$ Cu_3Pt

For $L1_2$ Cu_3Pt, MEAM-CEM/MC simulations (Fig. 4) and alloy surface energy calculations (Table V) both agree on a Cu termination of the (110) surface. The MEAM-CEM/MC prediction of a Cu termination is further supported by the DFT-PW91 (QE) and the MEAM-CEM segregation energies that exothermically favor segregation of Cu excess atoms to the equiatomic surface. The DFT-PW91 (QE) segregation energy of excess Pt to a pure Cu surface indicates that the (110) surface of $Cu_{3-\delta}Pt_{1+\delta}$ can accommodate more Pt atoms than suggested by the MEAM-CEM/MC simulations. Shen *et al.*[46] investigated the segregation behavior at the Cu_3Pt (110) surface with low energy ion spectroscopy (LEIS) and low energy electron diffraction (LEED). In contrast with the surface energy calculations, they reproducibly found a (110) surface that consists of 82% Cu with a virtually pure Cu second layer. The authors acknowledge that, at present, no quantitative theory seems to be able to reproduce their experimental result and to account for a difference in surface structure and ordering behavior in Cu_3Pt (100) and Cu_3Pt (110). The DFT, MEAM,[10] and MEAM-CEM calculations and simulations in this study cannot explain this phenomenon because a Cu enrichment of the equiatomic CuPt termination always induces segregation of Pt to the second layer. The large difference between the surface energy per atom of pure Cu and pure Pt (110) and the small effect of Pt strain energy in Cu_3Pt further sustain the prediction of a pure Cu (110) surface layer in Cu_3Pt.

At the (100) surface of $L1_2$ ordered Cu_3Pt, the MEAM-CEM/MC simulations also predict a pure Cu layer. DFT-LDA (QE) calculations confirm the Cu termination, but DFT-PW91 (QE) calculations rather give evidence for a CuPt termination (Table V). The segregation energies (Table VI) also point at this discrepancy: MEAM-CEM describes that excess Cu atoms segregate most exothermically to the surface and that Pt atoms do not, while DFT-PW91 (QE) segregation energies suggest that the pure Cu surface can accommodate at least some excess Pt atoms. However, the pure Cu surface termination is in excellent agreement with the LEIS and LEED measurements of Shen *et al.*,[47] who unambiguously measured a (1×1) Cu termination on top of a $c(2\times2)$ Cu-Pt second layer.

Below T_C, MEAM-CEM thus predicts that the low surface energy of Cu leads to a Cu-rich surface at the (100) and (110) surfaces of $L1_2$ Cu_3Pt. Above T_C, also a strong Cu segregation to these surfaces is observed, but the oscillations in the layer-by-layer composition profile are now limited to a few subsurface layers. These oscillations become smaller as T further increases. Such a subsurface profile is typical in alloys with attractive interatomic interactions and a pronounced surface segregation.[39]

For ordered $L1_2$ Cu_3Pt below T_C, the difference between pure Cu and pure Pt (111) surface energies is not sufficient to surpass the chemical interaction energy in the bulk. Segregation to the (111) surface of perfectly stoichiometric Cu_3Pt is then endothermic and thus entropy driven. At $T \ll T_C$, there is no significant surface segregation. As T approaches T_C and

the number of bulk antisite defects rises, the (111) surface evolves to 77.5% Cu and the second layer to 74.5%. For $T > T_C$, the faint and entropy-driven Cu segregation at the ordered (111) surface rapidly attenuates as the bulk order disappears. In stoichiometric Cu_3Pt, two segregation regimes to the (111) surface are thus recognized. Segregation is endothermic at rather low temperatures because the tradeoff between the lowering of the surface energy and the breakdown of the bulk order is endothermic. In this regime, segregation is proportional to the number of bulk antisite defects and increases with temperature. The other regime, at higher temperatures, is the exothermic segregation that lowers the surface energy from a disordered bulk. In off-stoichiometric $Cu_{3\pm\delta}Pt_{1\mp\delta}$, exothermic antisite induced surface segregation causes a substantial segregation of the excess species at low temperatures and diminishes at increasing temperatures. Shen *et al.*[48,49] studied Cu_3Pt (111) with LEIS and LEED and reported a slight enrichment of the surface layer to 80% Cu and a second layer that is depleted in Cu (69%), after annealing for 200 h at a temperature (800 K) close to the bulk order-disorder transition temperature (870 K).

Reference 10 gives a detailed description of the experimental evidence and the MEAM predictions on the surface segregation profile at the low index surfaces of Cu_3Pt. The MEAM results described in that paper are in excellent agreement with the MEAM-CEM results of this work. The prediction of the same segregation behavior illustrates the transferability of the MEAM-CEM formalism to anisotropic defects in alloys.

A recent LEED study[50] of Cu_3Pt (111), however, reports an unusual composition profile: Cu depletion at the surface (to 72%) and a significant Cu enrichment of the second layer (up to 92%). Tight binding Ising model (TBIM) calculations, presented in the same study, need two different sets of alloying pair interactions J_i in order to reproduce the stability of the $L1_1$ CuPt structure, with, on the one hand, $J_5=2J_2$ ($V_2=2V_1$) and, on the other hand, a smaller value of the ratio V_2/V_1 to reproduce the $L1_2$ Cu_3Pt structure. They investigated the segregation profile with the latter parameter set, both below and above T_C. These results are in good agreement with our MEAM-CEM/MC simulations. With the former parameter set, the authors suggest an $L1_1$-type bulk order profile in Cu_3Pt consisting of pure Cu planes and 50% Cu and 50% Pt planes alternating in the (111) direction. Of these two possible surface terminations in this hypothetical structure, according to TBIM, the pure Cu termination is the more stable. However, the corresponding surface profile agrees neither with the LEIS[48,49] profile nor with the LEED[50] results. The alternative, equiatomic termination is found to be only metastable within $45\% C_B < 70\%$ and unstable outside this region. Still, the authors suggested a satisfactory agreement with the LEED measurement. They suggested that the extended stability of this surface structure can be explained by contaminations that are supposed to favor Pt segregation. With the simulation results on surface segregation to the (111) surface of equiatomic CuPt [Fig. 5(c) and the next paragraph], it is now easier to understand the LEED results on (111) Cu_3Pt[50]. The Pt-rich (111) termination of a CuPt $L1_1$ compound can be a stable termination, even in the absence of contaminants.

2. $L1_1$ CuPt

Segregation is very pronounced at the (100) and (110) surfaces of the stoichiometric equiatomic CuPt alloy where the lower surface energy of Cu drives the Cu enrichment at $T < T_C$. The (110) surface of the stoichiometric $L1_1$ CuPt is even more Cu rich (±90% at 500 K) than the (100) surface (±80% at 500 K). This is explained by the larger difference of the surface energy per atom at the more open (110) surface than at the (100) surface. In stoichiometric equiatomic CuPt, this segregation increases as more bulk antisite defects are formed to reach a maximum close to T_C. Antisite induced surface segregation in $Cu_{1+\delta}Pt_{1-\delta}$ results in an exothermic segregation of excess Cu atoms to the (100) and (110) surfaces, resulting in a full Cu enrichment of the surface that decreases monotonously. Cu segregates endothermically at low temperature in $Cu_{1-\delta}Pt_{1+\delta}$. The (100) and (110) surfaces contain 50% Cu at ~300 K, but the number of Cu atoms in the surface rises as more Cu antisite defects are formed in the bulk alloy at increasing temperatures. The Cu concentration in both surfaces reaches a maximum close to T_C.

The stable Pt termination of the closer-packed (111) surface of $L1_1$ CuPt is explained by the release of elastic strain energy that surpasses the difference of the pure Cu and Pt surface energies. MEAM-CEM/MC simulations find the Pt termination stable on both Pt-rich and Cu-rich off-stoichiometric $Cu_{1\pm\delta}Pt_{1\mp\delta}$. Above T_C, Pt segregation to the (111) surface and Cu segregation to the (100) and (110) surfaces are exothermic and attenuate as T further increases.

To our knowledge, only theoretical evidence on the surface segregation in equiatomic CuPt alloys has been published. Khoutami *et al.*[51] and Senhaji *et al.*[52] described a TBIM investigation of the segregation profile. They reported a (90%) Cu termination at the (111) surface at $T > T_C$ and called it a surprising anisotropic effect compared to the (60%) Cu enrichment of the more open (100) surface at the same temperature. This is indeed surprising as one would expect a larger influence of the lower surface energy of Cu at the (100) surface than at the (111) surface. The authors attributed this anisotropy to the alloying effect in $L1_1$ CuPt. Our results on the (100) surface are in good agreement with their findings. This agreement, however, does not extend to the (111) surface. In Table V, both DFT-LDA (QE) and DFT-PW91 (QE) predictions sustain that a Pt termination is more stable than a Cu termination at the (111) surface of an $L1_1$ ordered CuPt alloy. The very exothermic DFT-PW91 (QE) and MEAM-CEM segregation energy of a Pt antisite to a Cu surface (Table VI) also strongly points to a Pt-rich (111) CuPt surface. In a theoretical $L1_0$-type alloy, DFT-LDA (QE) and DFT-PW91 (QE) confirm that a Cu termination is more stable than a Pt termination at the (100) surface, supporting Cu segregation to this surface. Here, a face-dependent segregation reversal is described for surfaces of the equiatomic CuPt alloy.

3. $L1_2$ $CuPt_3$

The lower surface energy of Cu compared to Pt also determines the surface segregation at the (110) surface of $L1_2$ $CuPt_3$ with a Cu-rich surface layer and a 100% Pt second layer. The stoichiometric ordered alloy displays a surface

with 45% Cu at 500 K. MEAM-CEM/MC simulations find that excess Cu (Pt) in the bulk induces exothermic Cu (Pt) segregation to the (110) surface but hardly influences the concentrations in the second layer. The DFT-PW91 (QE) segregation energies of excess Cu and Pt to the equiatomic CuPt surface (Table VI) suggest an even more Cu-rich (110) surface. The larger number of Pt atoms in the bulk $CuPt_3$ alloy leads to an increased influence of the strain energy, resulting in a face-related segregation reversal.

The segregation reversal is now situated between the (110) and (100) surfaces. Thus, at the (100) surface, an almost pure Pt layer terminates the $L1_2$ ordered alloy. Excess Cu atoms do not segregate to the pure Pt (100) surface so that off-stoichiometric $Cu_{1\pm\delta}Pt_{3\mp\delta}$ alloys also have a pure Pt (100) surface layer. This is also confirmed by the low MEAM-CEM and DFT-PW91 (QE) segregation energy of excess Cu to the pure Pt surface (Table VI). In MEAM-CEM/MC simulations, however, excess Cu atoms migrate to the second layer, while excess Pt atoms remain in the deeper layers below the surface.

At the (111) surface of ordered $L1_2$ $CuPt_3$, the release of the elastic strain of the larger Pt atoms and the chemical interactions induce an $L1_1$-like rearrangement of the three outermost surface layers. This results in a pure Pt surface and a sandwichlike subsurface with 66% Cu in the second layer. A surface region is formed, which is similar to the (111) surface of the equiatomic $L1_1$ CuPt alloy. The same surface profile was found at the (111) surface of Cu-rich and Pt-rich $Cu_{1\pm\delta}Pt_{3\mp\delta}$.

No experimental evidence on the surface segregation in $CuPt_3$ has yet been published. However, unpublished measurements[53] of the $CuPt_3$ (111) surface confirm a Pt enrichment of the surface layer. A possible $L1_1$-like surface rearrangement certainly deserves further attention. The segregation reversal between (100) and (110) surfaces is also indicated by the surface and segregation energy calculations of DFT-LDA (QE) and DFT-PW91 (QE): a stable Pt termination of the (100) surface, which is suggested by the low segregation energy of Cu to the pure Pt (100) surface, and a stable equiatomic (110) surface, which is suggested by the exothermic segregation energy of Cu to the pure Pt (110) surface (Table VI).

In conclusion, this discussion has shown that surface segregation in CuPt is mainly driven by the difference in surface energy between Cu and Pt. However, due to the smaller area per atom, this difference in surface energy presents a smaller driving force at the (111) and (100) surfaces, compared to the (110) surface, and the influence of strain energy becomes more important at surfaces of Pt-rich alloys. Both competing effects contribute to a face-dependent shift toward Pt segregation instead of the expected Cu segregation in CuPt between (100) and (111), and in $CuPt_3$ between (110) and (100).

VII. CONCLUSION

DFT parametrized MEAM potentials provide a consistent framework for the description of structural and compositional variations in metals and alloys, but MEAM overestimates the formation energy of ordered structures in which the number of interactions between different atomic species is maximized. This results in, for example, the prediction of an $L1_0$ rather than an $L1_1$ ground state for the equiatomic CuPt alloy.

The principal aim of this paper is to present a framework to further refine DFT-based MEAM calculations. A ground state correction of the MEAM is proposed through the addition of a limited number of cluster interactions as described in CEM. It now becomes possible to calculate the segregation profiles for different compositions, different surface orientations, and different temperatures, with only a small number of interaction parameters.

The main advantage is that the number of cluster interactions can straightforwardly be increased until the desired degree of accuracy for the ground state is achieved. On the other hand, MEAM adds structural information to CEM in order to describe anisotropic defects. A comparison with experimental results and additional DFT calculations of surface and segregation energies validates the results of the MEAM-CEM/MC simulations.

The stability of $L1_1$ in the equiatomic CuPt alloy, the amount of experimental and theoretical information, and the straightforward applicability of MEAM to transition metal alloys make CuPt an ideal alloy system to test the MEAM-CEM procedure. In the equiatomic CuPt alloy, an important correction is required for the MEAM method to adequately account for the greater stability of the $L1_1$ structure compared to $L1_0$. This essential correction could be achieved using a basic version of CEM to maintain the total complexity and parametrization effort comparable to the original MEAM. A large number of additional calculations were carried out to validate the MEAM-CEM parameter set: surface energies of pure Cu and Pt, bulk energies of several CuPt alloys, T_C of order-disorder transitions, surface energies of ordered CuPt alloys, and MC simulations of surface segregation profiles. The results are compared with experimental data from literature and with an independent set of DFT-LDA (QE) and DFT-PW91 (QE) calculations.

Reasoning on the "driving forces of segregation," an explanation is proposed for the observed surface segregation profiles, segregation energies, and surface energies of ordered CuPt alloys. The most remarkable result is the face dependence of the surface segregation in $Cu_{1\pm\delta}Pt_{1\mp\delta}$ and $Cu_{1\pm\delta}Pt_{3\mp\delta}$ alloys, where a subtle interplay of surface energy and release of elastic strain leads to a change in the segregating species. Cu segregates to the more open (100) and (110) surfaces of CuPt and to the (110) surface of $Cu_{3\pm\delta}Pt_{1\mp\delta}$, while Pt enriches the (111) surface of $Cu_{1\pm\delta}Pt_{1\mp\delta}$ and the (100) and (111) surfaces of $Cu_{1\pm\delta}Pt_{3\mp\delta}$. This face dependence was confirmed in this work with *ab initio* calculations.

ACKNOWLEDGMENTS

This work was supported by the Research Board of Katholieke Universiteit Leuven, the Research Foundation – Flanders, and the Research Board of Ghent University.

*Email address: Maarten.Schurmans@eu.umicore.com

[1] H. C. de Jongste and V. Ponec, J. Catal. **63**, 389 (1980).
[2] R. Linke, U. Schneider, H. Busse, C. Becker, U. Schröder, G. R. Castro, and K. Wandelt, Surf. Sci. **307-309**, 407 (1994).
[3] J. T. Kummer, J. Catal. **38**, 166 (1975).
[4] M. S. Daw and M. I. Baskes, Phys. Rev. B **29**, 6443 (1984).
[5] M. I. Baskes, Phys. Rev. B **46**, 2727 (1992).
[6] G. Bozzolo and J. Ferrante, Phys. Rev. B **50**, 5971 (1994).
[7] M. Aoki, Phys. Rev. Lett. **71**, 3842 (1993).
[8] D. B. Laks, L. G. Ferreira, S. F. Froyen, and A. Z. Zunger, Phys. Rev. B **46**, 12587 (1992).
[9] A. van de Walle and G. Ceder, Rev. Mod. Phys. **74**, 11 (2002).
[10] J. Luyten, M. Schurmans, C. Creemers, B. S. Bunnik, and G.-J. Kramer, Surf. Sci. **601**, 2952 (2007).
[11] M. Schurmans, J. Luyten, C. Creemers, and G. Bozzolo, Phys. Rev. B **72**, 064202 (2005).
[12] M. Schurmans, J. Luyten, and C. Creemers, Defect Diffus. Forum **263**, 129 (2007).
[13] J. Schiotz, F. D. Di Tolla, and K. W. Jacobsen, Nature (London) **391**, 561 (1998).
[14] J. G. Swadener, M. I. Baskes, and M. Nastasi, Phys. Rev. Lett. **89**, 085503 (2002).
[15] C. Creemers, P. Deurinck, S. Helfensteyn, and J. Luyten, Appl. Surf. Sci. **219**, 11 (2003).
[16] S. Helfensteyn, J. Luyten, L. Feyaerts, and C. Creemers, Appl. Surf. Sci. **212**, 844 (2003).
[17] S. Curtarolo, D. Morgan, and G. Ceder, CALPHAD: Comput. Coupling Phase Diagrams Thermochem. **29**, 163 (2005).
[18] S. Bärthlein, G. L. W. Hart, A. Zunger and S. Müller, J. Phys.: Condens. Matter **19**, 032201 (2007).
[19] J. P. Perdew, J. A. Chevary, S. H. Vosko, K. A. Jackson, M. R. Pederson, D. J. Singh, and C. Fiolhais, Phys. Rev. B **46**, 6671 (1992).
[20] G. Kresse and J. Furthmüller, Phys. Rev. B **54**, 11169 (1996).
[21] G. Kresse and J. Furthmüller, Comput. Mater. Sci. **6**, 15 (1996).
[22] J. P. Perdew and A. Zunger, Phys. Rev. B **23**, 5048 (1981).
[23] S. Baroni *et al.*, http://www.pwscf.org/
[24] D. Vanderbilt, Phys. Rev. B **41**, 7892 (1990).
[25] P. R. Subramanian and D. E. Laughlin, in *Binary Alloy Phase Diagrams*, 2nd ed., edited by T. B. Massalski (American Society for Metals, Ohio, 1990), Vol. 2.
[26] V. Blum, G. L. W. Hart, M. J. Walorski, and A. Zunger, Phys. Rev. B **72**, 165113 (2005).
[27] J. M. Sanchez, F. Ducastelle, and D. Gratias, Physica A **128**, 334 (1984).
[28] A. Zunger, in *Statics and Dynamics of Alloy Phase Transformations*, NATO Advanced Studies Institute, B: Physics, edited by P. E. A. Turchi and A. Gonis (Plenum, New York, 1994), p. 361.
[29] S. Muller, J. Phys.: Condens. Matter **15**, R1429 (2003).
[30] G. L. W. Hart, V. Blum, M. Walorski, and A. Zunger, Nat. Mater. **4**, 391 (2005).
[31] H. Y. Geng, M. H. F. Sluiter, and N. X. Chen, Phys. Rev. B **73**, 012202 (2006).
[32] J. W. D. Connolly and A. R. Williams, Phys. Rev. B **27**, 5169 (1983).
[33] N. Metropolis, A. W. Rosenbluth, M. N. Rosenbluth, A. H. Teller, and E. Teller, J. Chem. Phys. **21**, 1087 (1953).
[34] J. M. Cowley, Phys. Rev. **77**, 669 (1950).
[35] K. Rapcewicz, B. Chen, B. Yakobson, and J. Bernholc, Phys. Rev. B **57**, 7281 (1998).
[36] A. V. Ruban, Phys. Rev. B **65**, 174201 (2002).
[37] L. V. Pourovskii, A. V. Ruban, B. Johansson, and I. A. Abrikosov, Phys. Rev. Lett. **90**, 026105 (2003).
[38] P. Wynblatt and R. C. Ku, Surf. Sci. **65**, 511 (1977).
[39] C. Creemers, S. Helfensteyn, J. Luyten, and M. Schurmans, in *Applied Computational Materials Modeling: Theory, Experiment, and Simulations*, edited by G. Bozzolo, P. Abel, and R. D. Noebe (Kluwer Academic, New York, 2006).
[40] W. B. Pearson, *A Handbook of Lattice Spacings and Structures of Metals and Alloys* (Pergamon, Oxford, 1958).
[41] J. Emsley, *The Elements* (Clarendon, Oxford, 1991).
[42] *Handbook of Chemistry and Physics*, edited by D. R. Lide (CRC, Boca Raton, FL, 1992).
[43] W. R. Tyson and W. A. Miller, Surf. Sci. **62**, 267 (1977).
[44] F. R. de Boer, R. Boom, W. C. M. Mattens, A. R. Miedema, and A. K. Niessen, in *Cohesion and Structure*, edited by F. R. de Boer and D. G. Pettifor (North-Holland, Amsterdam, 1988), Vol. 1.
[45] F. L. Williams and D. Nason, Surf. Sci. **45**, 377 (1974).
[46] Y. G. Shen, D. J. O'Connor, and K. Wandelt, Surf. Sci. **410**, 1 (1998).
[47] Y. G. Shen, D. J. O'Connor, and K. Wandelt, Surf. Sci. **406**, 23 (1998).
[48] Y. G. Shen, D. J. O'Connor, and R. J. MacDonald, Solid State Commun. **96**, 557 (1995).
[49] Y. G. Shen, D. J. O'Connor, K. Wandelt, and R. J. MacDonald, Surf. Sci. **331-333**, 746 (1995).
[50] Y. Gauthier, A. Senhaji, B. Legrand, G. Tréglia, C. Becker, and K. Wandelt, Surf. Sci. **527**, 71 (2003).
[51] A. Khoutami, B. Legrand, and G. Treglia, Surf. Sci. **287-288**, 851 (1993).
[52] A. Senhaji, G. Treglia, and B. Legrand, Surf. Sci. **307-309**, 440 (1994).
[53] C. Becker, T. Pelster, M. Tanemura, J. Breitbach, and K. Wandelt, Surf. Sci. **427-428**, 403 (1999).